

## THE ULTRAVIOLET SPECTRUM AND CONTINUUM ENERGY DISTRIBUTION OF THE BRIGHT QUASAR H1821+643

MICHEL KOLMAN & JULES P. HALPERN<sup>1</sup>

Columbia Astrophysics Laboratory, Columbia University, 538 West 120th Street, New York, NY 10027

CHRIS R. SHRADER<sup>2</sup>

Astronomy Programs, Computer Sciences Corporation

AND

ALEXEI V. FILIPPENKO<sup>1,3</sup>

Astronomy Department, University of California, Berkeley, CA 94720

Received 1990 August 20; accepted 1990 November 9

### ABSTRACT

We report on the first UV observations of the bright QSO H1821+643. With  $V = 14.2$  mag and  $z = 0.297$ , H1821+643 is the second brightest object in the sky at  $z > 0.1$ . The *IUE* data are combined with new optical spectroscopy, and existing infrared and X-ray data, to reveal a strong optical/UV “big bump,” which continues past the Lyman limit in the rest frame of the QSO. A possible turnover at the high-frequency side of the UV continuum constrains fits of a thin accretion disk model to a large black hole mass ( $M \simeq 3 \times 10^9 M_{\odot}$ ) and high accretion rate ( $\dot{M} \simeq 19 M_{\odot} \text{ yr}^{-1}$ ), but a small disk size ( $R_{\text{out}}/R_{\text{in}} \simeq 12$ ). The shape of the UV continuum was found to be variable, with a hardening of the spectrum when the source was brighter. Because of its location only  $3^{\circ}$  from the ecliptic pole, H1821+643 will be an important object for simultaneous UV and soft X-ray monitoring to test for a common origin of the UV bump and soft X-ray excess.

*Subject headings:* quasars — spectrophotometry — ultraviolet: spectra

### 1. INTRODUCTION

Twenty years after the discovery of QSOs, one of the brightest objects of this class had yet to be noticed. Known as H1821+643, it was identified by Pravdo & Marshall (1984) as the counterpart of an X-ray source first detected by *HEAO 1* and then by *Einstein*. With  $V = 14.2$  mag, it is the brightest object after 3C 273 at  $z > 0.1$ . The brighter members of a class often contribute disproportionately to our knowledge of their physics, because they can be studied well at many wavelengths. The intermediate redshift of H1821+643 ( $z = 0.297$ ) makes it well-suited to a study of the intrinsic ultraviolet continuum, as higher redshift objects suffer from absorption by intergalactic H I clouds. Moreover, its location only  $3^{\circ}$  from the ecliptic pole [the position is  $\alpha(1950) = 18^{\text{h}}21^{\text{m}}41^{\text{s}}.67$ ,  $\delta(1950) = 64^{\circ}19'0''.8$ ] makes H1821+643 an important object for monitoring programs done with satellites. In particular, it is an ideal object to test for a common origin of the UV big bump and the soft X-ray excess, an association which has yet to be proven.

In this paper, we report new ultraviolet and optical spectrophotometry which we combine with existing infrared and X-ray data to study the continuum energy distribution of this QSO. The combined optical and *IUE* spectra show a strong UV bump. The moderate redshift allows the detection of flux past the Lyman limit in the rest frame, while allowing for optimal coverage of the UV bump within the *IUE* bandpass. We present fits to a thin disk model, which require large mass and accretion rate for this high luminosity QSO, but also indicate a small outer radius for the disk.

The strong soft X-ray excess, which was attributed to H1821+643 in the *HEAO A-2* data of 1977, is absent in all

subsequent X-ray observations, which resemble the “canonical” hard power law. Although we take this variable soft excess at face value for the purpose of this paper, we also discuss other soft X-ray sources in the vicinity of the QSO which could have confused the *HEAO A-2* low-energy detector.

### 2. OBSERVATIONS

#### 2.1. The X-Ray Identification

When H1821+643 was identified by the *Einstein* imaging proportional counter (IPC), comparison with *HEAO A-2* data obtained 3 yr earlier indicated that a factor of 4 decrease in the soft X-ray flux had occurred between 1977 and 1980 (Pravdo & Marshall 1984). The change could be described as the disappearance of the soft X-ray excess, which is clearly present in the *HEAO A-2* low energy detector (LED), and not evident in the *Einstein* IPC. Subsequent observations by *EXOSAT* in 1984 and 1985 (Warwick, Barstow, & Yaqoob 1989) also did not detect a soft X-ray excess, leading these authors to consider the possibility that the *HEAO A-2* LED detector had been confused by another soft X-ray source in the field, possibly the central star of the planetary nebula K1-16 (Grauer & Bond 1984) which is  $100''$  from the QSO. But having estimated the flux from K1-16 in the 0.2–2 keV bandpass of the LED, Warwick et al. (1989) concluded that it could not have contributed significantly to the observed soft X-ray excess.

We can further address this issue with the *Einstein* IPC data since the IPC bandpass includes that of the *HEAO A-2* LED. Moreover, the IPC data were taken as part of a survey of the north ecliptic pole region, which can be searched for other soft X-ray sources in the vicinity of the LED error box. There were four overlapping fields, all of which included H1821+643, although in three of these the QSO fell just outside the support ribs of the detector, hampering detailed quantitative analysis.

<sup>1</sup> Guest Observer with the *International Ultraviolet Explorer* Satellite.

<sup>2</sup> Staff member, *IUE* Observatory, NASA/GSFC. Postal address: Code 668.1, NASA/GSFC, Greenbelt, MD 20771.

<sup>3</sup> Presidential Young Investigator.

The X-ray position and pointlike nature of the source in the IPC map are consistent with identification with the QSO and not the planetary nebula, although it cannot be excluded that K1-16 might make a small contribution to the IPC X-ray source. More worrisome for the interpretation of the soft excess in the LED is another X-ray source 36' to the northeast of the QSO, which is of comparable intensity. We identified this source with the 8.0 mag K0 star, SAO 17878. The error boxes of the several *HEAO-1* detectors, in addition to the optical positions of possible confusing sources, are shown in Figure 1. The X-ray flux of SAO 17878 in the 0.1–3.5 keV band as observed with the IPC is  $9 \times 10^{-12}$  ergs  $\text{cm}^{-2} \text{s}^{-1}$ , about half that of the QSO at the time of the *Einstein* observations. In the absence of detailed knowledge about its variability, it cannot be ruled out that this star contaminated the LED error box (Nugent et al. 1983), on whose edge it lies. However, the X-ray flux from this star would have to have been at least 4 times larger than the *Einstein* value for it to have made a substantial contribution to the LED flux. The only other X-ray source close to the LED error box is a 5.0 mag F5 star, SAO 17828, with an IPC flux of about  $1 \times 10^{-12}$  ergs  $\text{cm}^{-2} \text{s}^{-1}$ . This source is an even less likely contributor. In summary, we can be certain that the hard X-rays arose in the QSO, as indicated by the IPC source and the small *HEAO A-1* error box of  $0.05 \text{ deg}^2$  (Wood et al. 1984). We can also be certain that the soft excess was not present during the *Einstein* or *EXOSAT* observations. Whether the soft excess observed by the *HEAO A-2* LED arose exclusively in the QSO cannot be determined, although this appears highly likely.

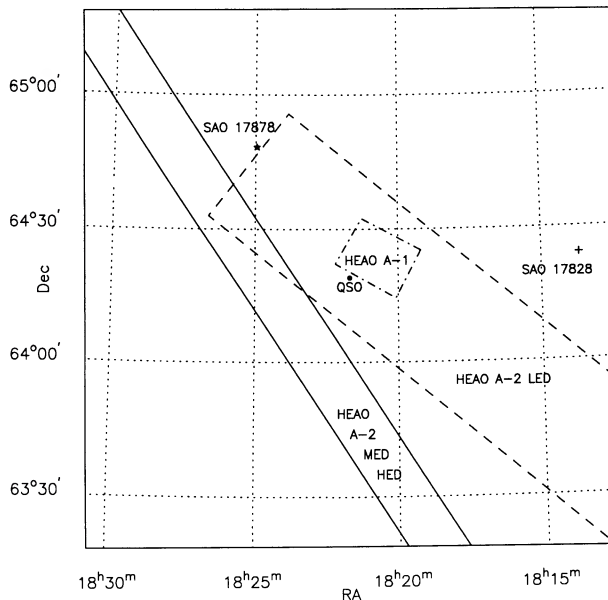


FIG. 1.—Error boxes of the *HEAO* observations around H1821+643 (indicated by the filled circle labeled QSO). The *HEAO A-2* MED-HED error box (Marshall et al. 1979) is indicated by the solid lines; the *HEAO A-2* LED error box (Nugent et al. 1983) is indicated by the dashed lines; the *HEAO A-1* error box (Wood et al. 1984) is indicated by the dot-dashed lines. The star indicates the position of SAO 17878, which could contribute some of the detected flux in the *HEAO A-2* LED band. The plus sign indicates the position of the weak IPC source SAO 17828. The IPC error circles for the QSO and SAO stars have a typical diameter of 1' and are too small to be drawn in this figure. All positions are in 1950 coordinates.

TABLE 1  
EINSTEIN IPC SPECTRUM OF H1821+643

Date	1980 May 25
Exposure time (s)	960.0
IPC counts $\text{s}^{-1}$ (0.1–3.9 keV)	$0.508 \pm 0.023$
$F_x$ (0.1–3.5 keV) <sup>a</sup>	$1.74 \times 10^{-11}$
$L_x$ (0.1–3.5 keV) <sup>b</sup>	$9.6 \times 10^{45}$
$A^c$	$4.23 \times 10^{-3}$
$\alpha$ (68% confidence)	$0.60 \pm 0.34$
(90% confidence)	(+0.62, -0.45)
$N_H$ ( $\text{cm}^{-2}$ ) (68% confidence)	$2.0 (+1.8, -1.5) \times 10^{20}$
(90% confidence)	$< 5.0 \times 10^{20}$
$\chi^2_{\text{min}}$ (per d.o.f.)	1.34

<sup>a</sup> Flux (ergs  $\text{cm}^{-2} \text{s}^{-1}$ ) in observed energy band.

<sup>b</sup> Luminosity (ergs  $\text{s}^{-1}$ ) in intrinsic energy band, corrected for absorption and assuming  $\alpha = 0.6$ ,  $H_0 = 50 \text{ km s}^{-1} \text{ Mpc}^{-1}$ , and  $q_0 = 0$ .

<sup>c</sup> Normalization constant.

## 2.2. The X-Ray Spectrum

We performed a standard spectral analysis on the single *Einstein* IPC observation in which the QSO fell inside the support ribs. The results are listed in Table 1. Power-law fits yielded a best-fit energy index  $\alpha = 0.6$ , with 68% confidence limits of 0.26–0.94, and 90% confidence limits of 0.15–1.12. The 90% upper limit on the column density  $N_H$  is  $5 \times 10^{20} \text{ cm}^{-2}$ , which is consistent with the 21 cm value of  $4.1 \times 10^{20} \text{ cm}^{-2}$  (Stark et al. 1990). Hard X-ray spectral measurements by *EXOSAT* (Warwick et al. 1989) and *Ginga* (Turner et al. 1989; Kii et al. 1991) are consistent with an extrapolation of the IPC data, both in spectral index and normalization. Therefore, it seems likely that the soft excess observed by the *HEAO A-2* LED is a separate component, which varies independently of the hard power law.

## 2.3. The Ultraviolet Observations

In 1987 we obtained the first UV spectra of H1821+643 with the *IUE* satellite. The strong and broad Lyman- $\alpha$  emission line was saturated in the 300 minute exposure of the SWP. A subsequent shorter exposure (120 minutes) resulted in optimal detection in the Lyman- $\alpha$  line. All the *IUE* observations are listed in Table 2. The images were obtained with the large aperture in the low-dispersion mode, resulting in a spectral resolution of about 5 Å and about 8 Å for the SWP and LWP, respectively.

The spectra were obtained from the line-by-line images with the Gaussian extraction routines at the Goddard Regional Data Analysis Facility to minimize the noise while maintaining accurate flux levels. We corrected the spectra for the effects of interstellar reddening, using the extinction curve of Seaton (1979) and  $E(B-V) = 0.085 \text{ mag}$ . The color excess is based on

TABLE 2

*IUE* OBSERVATIONS OF H1821+643

Image	Int. time (minutes)	Date
SWP 31431 .....	300	1987 Jul 29
LWP 11294 .....	130	1987 Jul 29
SWP 31523 .....	120	1987 Aug 10
SWP 35516 .....	275	1989 Feb 9
LWP 14996 .....	95	1989 Feb 9
SWP 36396 .....	300	1989 Jun 4
LWP 15659 .....	120	1989 Jun 4

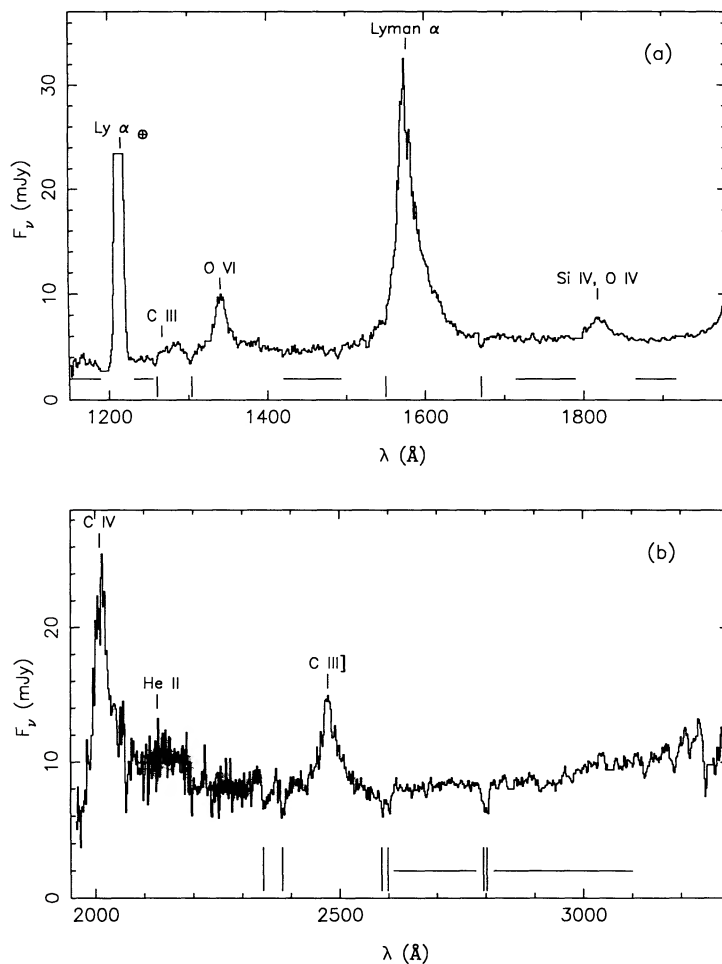


FIG. 2.—(a) Co-added SWP spectrum of H1821+643 obtained with *IUE*, corrected for the estimated interstellar extinction of  $E(B-V) = 0.085$  mag. The Lyman- $\alpha$  emission is patched in from the unsaturated image, SWP 31523. (b) LWP spectrum. The horizontal lines denote the wavelengths selected as the continuum and used in Figs. 4 and 6. The vertical tick marks indicate the detected interstellar absorption lines.

the neutral hydrogen column density in the direction of H1821+643 ( $N_{\text{H}} = 4.1 \times 10^{20} \text{ cm}^{-2}$ , Stark et al. 1990) and the  $N_{\text{H}}/E(B-V)$  ratio of  $4.8 \times 10^{21} \text{ cm}^{-2} \text{ mag}^{-1}$  (Bohlin, Savage, & Drake 1978). We did not correct for any internal reddening, as there is now growing evidence that the intrinsic extinction in QSOs is very small (Sun & Malkan 1989a, and references therein). We deleted the data points which were flagged because of the presence of a resseau. The co-added spectrum is shown in Figure 2. The overall continuum level decreases slightly with increasing frequency. The flux level is sensitive to the correction for interstellar extinction, but even if the spectrum is overcorrected for reddening [up to  $E(B-V) = 0.2$  mag], a downward trend with shorter wavelengths remains. Despite the decline in sensitivity below 1200 Å, there is strong emission shortward of the Lyman limit, which is redshifted to 1182 Å (Fig. 3).

As listed in Table 2, there are three series of observations with *IUE*, each resulting in at least one SWP and LWP image: the first in 1987, the second in 1989 February, and the third in 1989 June. Two SWP spectra were obtained in 1987: a long exposure with optimal detection of the continuum level and a short exposure with optimal detection of the Lyman- $\alpha$  emission line. In order to study the continuum, the spectra were binned into about 10 data points per camera, avoiding the

major emission lines and the Galactic absorption lines. If we compare these three series of observations, no significant changes could be found between the first and second series, while the spectral shape did change significantly between the second and third series. As shown in Figure 4, the emission between 2000 and 3000 Å decreased in intensity, while the short wavelength side increased by about 10%, resulting in a hardening of the spectrum between 1989 February and June.

#### 2.4. Optical Spectroscopy

Optical CCD spectra of H1821+643 covering the wavelength range 3138–10046 Å were obtained on 1988 October 3 UT using four different grating settings of the UV Schmidt spectrograph (Miller & Stone 1987) at the Cassegrain focus of the Shane 3 m reflector at Lick Observatory. The spectra were obtained through a long slit of width 8", oriented along the parallactic angle (Filippenko 1982). The airmass was 1.3, conditions were photometric, and the seeing was about 1". Typical integration times per setting were 300–500 s. The spectral resolution was 5–8 Å below about 7200 Å, and 10–16 Å in the near-IR region.

Standard techniques were used to extract one-dimensional spectra from the CCD data. These included subtraction of the bias level, division by a flat field, removal of cosmic rays, cor-

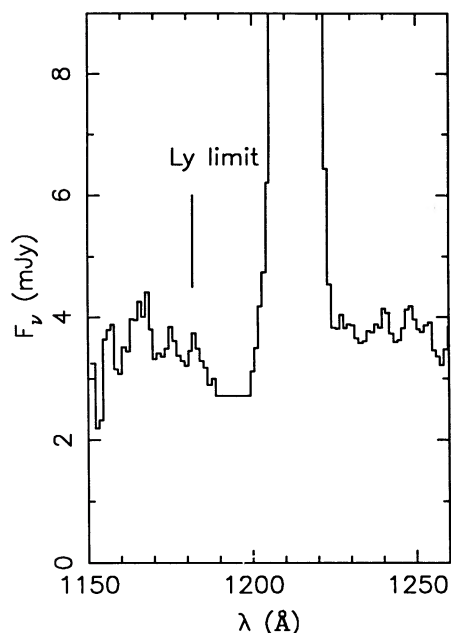


FIG. 3.—Expanded view of Fig. 2a shows the presence of substantial flux below the Lyman limit at 1182 Å (indicated by the vertical tick-mark). We estimate that the covering fraction at the Lyman limit must be less than 0.09. The strong emission line around 1216 Å is geocoronal Lyman- $\alpha$ . The data points around 1190 Å are deleted because of the presence of reseau.

rection for geometric distortion and misalignments, and subtraction of the background sky. Several stars from the lists of Oke & Gunn (1983) and Massey et al. (1988) were used to flux calibrate the spectra, as well as to remove telluric absorption bands at wavelengths longer than 6200 Å. Excellent agreement in absolute fluxes and spectral shapes was found in overlapping spectral regions. However, the wavelength scale is uncertain by about 4 Å, since the observations were obtained through a wide slit. The redshift derived from the [O III] lines is  $0.2972 \pm 0.0006$ .

The overall optical spectrum of H1821+643, corrected for extinction [ $E(B-V) = 0.085$  mag], is shown in Figure 5. The near-UV flux joins that of the *IUE* spectrum very well, as can be seen by comparison of Figures 2 and 5.

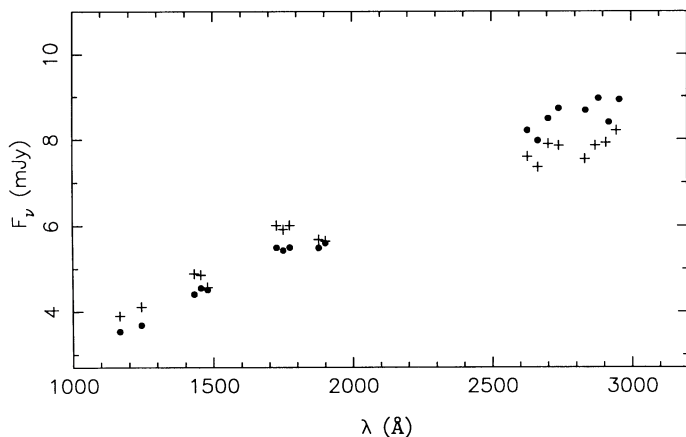


FIG. 4.—Change in the UV continuum shape between 1989 February 9 (indicated by filled circles) and 1989 June 4 (indicated by plus signs). The flux increased by about 10% at the shortest wavelengths while the flux decreased at the long-wavelength side, corresponding to a hardening of the spectrum.

## 2.5. Optical and Infrared Photometry

The *UBV* photometry was obtained by S. Vrtilek with the 0.9 m telescope at Kitt Peak National Observatory on 5 nights centered around 1988 October 10. Variability in the *V* band was less than 0.03 mag from night to night, and less than 0.04 mag and 0.2 mag for *B-V* and *U-B*, respectively. The average magnitudes are listed in Table 3. Near infrared magnitudes from the Infrared Telescope Facility (IRTF) in the *J* (1.25  $\mu$ m), *H* (1.65  $\mu$ m), *K* (2.2  $\mu$ m), and *L'* (3.8  $\mu$ m) bands were provided by M. Elvis, and are listed in Table 3. In the far infrared, *IRAS* detections in all four bands were published by Neugebauer et al. (1986), and are also listed in Table 3.

The overall continuum distribution derived from all the above data and shifted to the rest-frame is shown in Figure 6. Throughout this article  $\lambda$  and  $\nu$  denote observed wavelength and frequency, while  $\lambda_0$  and  $\nu_0$  denote the wavelength and frequency in the rest-frame of the QSO.

## 2.6. Radio Observations

VLA observations at 6 cm with a partial array of six dishes and an exposure time of 20 minutes yielded an upper limit of 15 mJy, establishing this QSO as radio quiet.

## 3. RESULTS

### 3.1. Emission Shortward of the Lyman limit

The redshift of H1821+643 (0.297) is high enough to shift the Lyman limit to 1182 Å, into the wavelength range of *IUE*, but low enough to avoid absorption by intervening H I clouds. Substantial flux is detected below 1182 Å in all our SWP spectra (Fig. 2). An upper limit to the covered fraction of the continuum source as derived from the flux levels below and above 1182 Å is estimated at 0.09; a small value consistent with the absence of X-ray absorption in this and other bright AGNs. This small covering fraction of less than 0.1 is also expected in a high luminosity QSO such as H1821+643 on the basis of photon counting arguments concerning the photoionization of clouds on the BLR. Rest-frame Lyman continuum absorption has been reported (Kinney et al. 1985) in less than 10% of all AGNs. Another bright QSO, 3C273, is a possible

TABLE 3  
PHOTOMETRY OF H1821+643

Band	Magnitude	Flux (mJy)
U <sup>a</sup> .....	13.30	9.04
B <sup>a</sup> .....	14.30	8.12
V <sup>a</sup> .....	14.26	7.55
J <sup>b</sup> .....	13.09	8.8
H <sup>b</sup> .....	12.19	13.0
K <sup>b</sup> .....	11.12	22.1
L <sup>b</sup> .....	8.95	60.5
12 $\mu$ m <sup>c</sup> .....		236
25 $\mu$ m <sup>c</sup> .....		373
60 $\mu$ m <sup>c</sup> .....		953
100 $\mu$ m <sup>c</sup> .....		2164
6 cm .....		< 15

<sup>a</sup> Magnitude averaged over 5 nights, obtained with the automated filter photometer on the 0.9 m telescope at Kitt Peak National Observatory around 1988 October 10 (S. Vrtilek 1988, private communication).

<sup>b</sup> IRTF instrumental magnitude, obtained with 6" diameter aperture and the InSb detector (RC2) on 1988 April 25 (M. Elvis 1988, private communication).

<sup>c</sup> *IRAS* fluxes (Neugebauer et al. 1986).

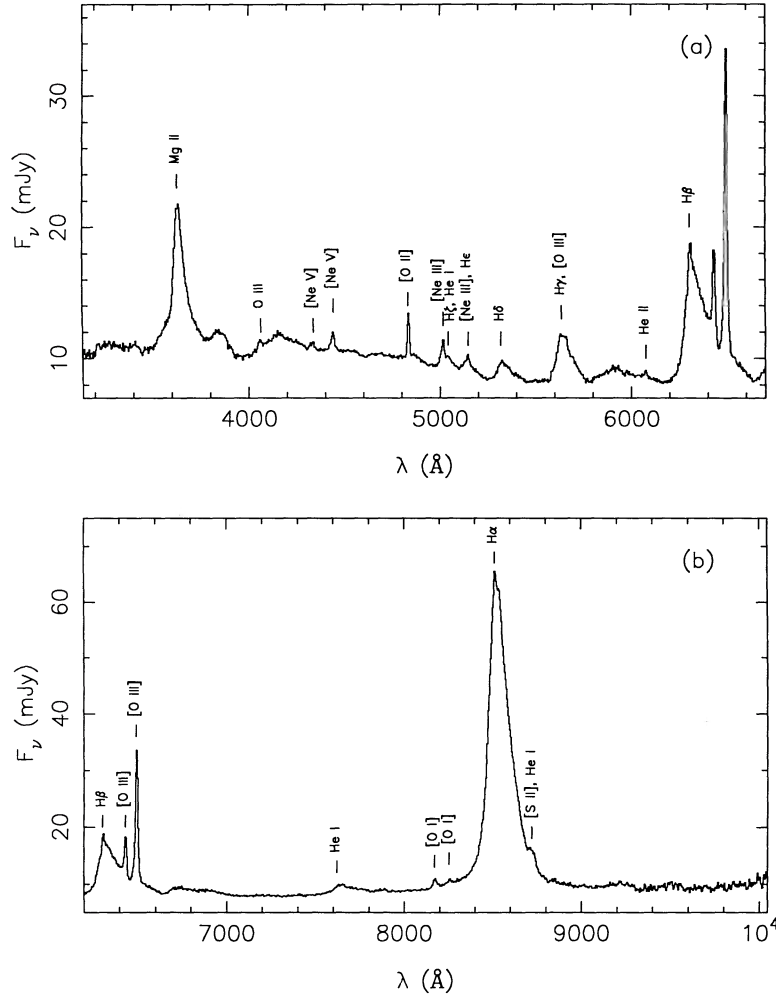


FIG. 5.—Optical spectrum of H1821+643 obtained at Lick Observatory on 1988 October 3 under photometric conditions. The interstellar extinction correction for  $E(B-V) = 0.085$  mag has been applied. The continuum appears bumpy due to the contribution of blended Fe II lines (e.g., around 3800, 4200, 5900, and 6700 Å).

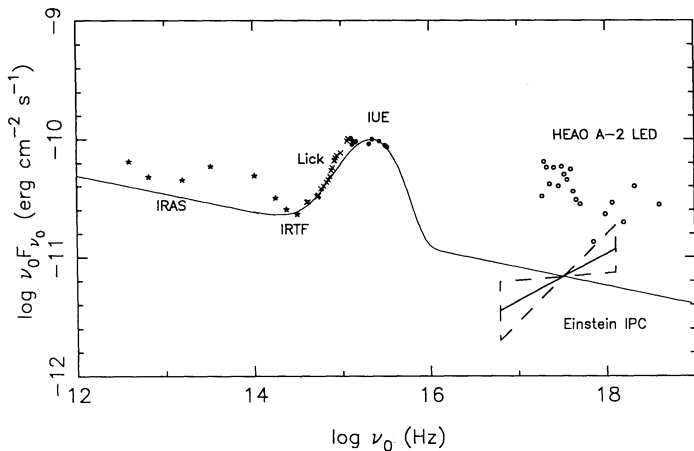


FIG. 6.—Overall continuum spectrum of H1821+643 plotted in the QSO rest frame, with the co-added IUE data from 1987. Note the turnover of the UV bump and the large amplitude variation between the X-ray observations. The power-law plus thin accretion disk (solid line) fit with  $M = 3 \times 10^9 M_{\odot}$ ,  $\dot{M} = 19 M_{\odot} \text{ yr}^{-1}$ , and  $R_{\text{out}}/R_{\text{in}} = 12$ , deviates between  $\log \nu_0 = 14.8$  and  $\log \nu_0 = 15.2$  due to the Balmer continuum and Fe II line emission.

exception, as a Lyman discontinuity has been reported in combined IUE/Voyager data (Reichert et al. 1988). By contrast, the continuum spectrum of H1821+643 seems to turn over smoothly well longward of the Lyman limit, which argues that the thermal peak, rather than any Lyman limit absorption, is responsible for the drop in flux level at the high-frequency side of the IUE spectrum. However, one must be aware of the possibility that Lyman continuum absorption is an intrinsic property of accretion disks in AGNs (Sun & Malkan 1987; Sun & Malkan 1989b; Scott & O'Dell 1989), and that a suitable smearing of the Lyman edge due to strong Doppler and gravitational effects in the inner disk might cause some of the turnover which is observed.

### 3.2. Continuum Energy Distribution

None of the observations in different wavebands were simultaneous; nevertheless, the infrared through UV data are very continuous. There is a steep rise in the flux level at optical frequencies, and the IUE data points indicate a strong UV bump. The prominence of the UV bump is similar to the one detected in the optical/UV bump prototype PG 1211+143, but it could be observed to higher rest-frame frequencies due to the higher redshift ( $z = 0.297$  vs.  $z = 0.085$  for PG 1211+143).

In all the spectra except the one obtained in 1989 June, there is evidence for a turnover at the high-frequency side (around  $\log \nu_0 = 15.3$ ).

Because of the  $5 \mu\text{m}$  feature displayed by the IR data points, the power law, if any, is not well defined in the infrared. By forcing a fit to the  $60 \mu\text{m}$  and  $1 \mu\text{m}$  data points, we find  $\alpha = 1.16$  (where  $F_\nu \propto \nu^{-\alpha}$ ). Because there is a strong correlation between the IR and hard X-rays in QSOs (Edelson & Malkan 1986; Kriss 1988), a single power law might be extrapolated from  $\log \nu_0 \approx 12$  to  $\log \nu_0 \approx 18$ . The turn-up from the overall power law of the hard X-ray data (both for the *Einstein* data and the 2–10 keV *HEAO 1* data) is typical for the high-frequency side of the continuum energy distribution in QSOs (Elvis 1988). Considering the large amplitude of variability in the X-rays, it is impossible to estimate the soft X-ray flux level at the time of the *IUE* observations, which would be important for models of the soft X-ray excess.

### 3.3. Emission Lines

Information on continuum emission in the unobservable EUV gap can be derived from the UV and optical emission lines, which are powered by photons with EUV energies. To this end, we measured the major emission lines in the UV and optical spectra. No significant differences in line fluxes were found from one *IUE* observation to the other; therefore, all the *IUE* spectra were coadded and dereddened. The measured line properties are listed in Table 4 and the lines are identified in Figures 2 and 5. The Lyman- $\alpha$  emission line could only be

TABLE 4  
EMISSION-LINE MEASUREMENTS OF H1821+643

ID <sup>a</sup>	Intensity <sup>b</sup>	Flux <sup>c</sup>	EW <sup>d</sup> (Å)
C III $\lambda 977$ .....	<35.0	<20.3	<5.0
O VI $\lambda 1034^e$ .....	137.1	83.4	16.8
Ly $\alpha$ $\lambda 1216$ , (N V $\lambda 1240$ ) .....	963.5	626.9	156.0
Si IV $\lambda 1397$ , O IV $\lambda 1407$ .....	49.8	32.8	10.0
C IV $\lambda 1549$ .....	504.8	305.9	111.4
He II $\lambda 1640$ , (O III] $\lambda 1663$ ) .....	161.9	91.7	36.8
C III] $\lambda 1909$ .....	115.2	78.1	30.4
Mg II $\lambda 2798$ .....	222.6	186.5	98.7
O III $\lambda 3133$ .....	1.8	1.6	1.0
[Ne V] $\lambda 3345$ .....	2.1	1.8	1.3
[Ne V] $\lambda 3426$ .....	4.3	3.8	2.8
[O II] $\lambda 3727$ .....	5.1	4.6	4.1
[Ne III] $\lambda 3869$ .....	4.5	4.2	4.7
H $\zeta$ $\lambda 3889$ , He I $\lambda 3888$ .....	2.4	2.2	2.5
[Ne III] $\lambda 3968$ , He $\lambda 3970$ .....	3.6	3.3	3.6
H $\delta$ $\lambda 4102$ .....	11.0	10.3	13.2
H $\gamma$ $\lambda 4340$ , [O III] $\lambda 4363$ .....	29.0	27.8	39.3
He II $\lambda 4686$ .....	0.6	0.6	1.0
H $\beta$ $\lambda 4861$ .....	100.0	100.0	172.6
[O III] $\lambda 4959$ .....	8.4	8.3	10.4
[O III] $\lambda 5007$ .....	28.6	28.4	40.3
He I $\lambda 5876$ .....	9.8	10.2	24.0
[O I] $\lambda 6300$ .....	1.6	1.7	4.0
[O I] $\lambda 6363$ , ([Fe X] $\lambda 6375$ ) .....	0.9	0.9	2.0
H $\alpha$ $\lambda 6563$ , ([N II] $\lambda \lambda 6548, 83$ ) .....	333.3	352.3	895.1
[S II] $\lambda 6716, 30$ (He I $\lambda 6678$ ) .....	4.8	5.1	9.9

<sup>a</sup> Identification of emission line and rest wavelength; the lines in parentheses denote only minor contributions.

<sup>b</sup> Intensity corrected for Galactic reddening, relative to H $\beta$ , with  $I(\text{H}\beta) = 1.05 \times 10^{-12} \text{ ergs cm}^{-2} \text{ s}^{-1}$ .

<sup>c</sup> Observed flux relative to H $\beta$  with  $F(\text{H}\beta) = 8.63 \times 10^{-13} \text{ ergs cm}^{-2} \text{ s}^{-1}$ .

<sup>d</sup> Observed equivalent width.

<sup>e</sup> Narrow component only (FWOI  $\sim 40 \text{ \AA}$ ).

measured in SWP 31523, as the other SWP spectra were saturated at this line. The major source of error in the line measurements is the uncertainty in the continuum level, which is contaminated by the broad wings of the emission lines, Galactic absorption lines, and blended Fe II line and Balmer continuum emission. For the O VI  $\lambda 1034$  emission line only the narrow component was measured (with a full width at zero intensity, FWOI, of about  $40 \text{ \AA}$ ), as it was unclear to where the broad wings extend (possibly from  $1280$  to  $1380 \text{ \AA}$ , encompassing the Galactic absorption feature around  $1300 \text{ \AA}$ ). This uncertainty around the O VI line also complicated the measurement of the upper limit to C III  $\lambda 977$  at its redshifted wavelength of  $1267 \text{ \AA}$ , as well as the measurement of the O I  $\lambda 1302$ , Si II  $\lambda 1304$  absorption feature.

These UV observations are the first to be conducted for H1821+643. There were, however, previous optical observations with emission line measurements from 1981 (Pravdo & Marshall 1984). The equivalent widths listed by these authors for Mg II, H $\gamma$  and H $\beta$  are smaller (by about 30%) than our measurements, and larger (by 15%) for [O III]  $\lambda 5007$ . Compared to a sample of 20 intermediate redshift QSOs ( $z < 0.84$ , Kinney et al. 1985) the EW of Lyman- $\alpha$  for H1821+643 is typical, being close to the sample's average. Kwan & Krolik (1981) compiled the average and range of permitted line ratios for a large sample of QSOs. No single line ratio observed in H1821+643 is outside this sample's range. Compared to the mean, the observed ratios of Ly $\alpha$ /H $\beta$ , C IV  $\lambda 1549$ /Ly $\alpha$ , and Mg II  $\lambda 2798$ /H $\beta$  in H1821+643 are large (by a factor of about 1.5), while the C III]  $\lambda 1909$ /C IV  $\lambda 1549$  ratio is half the mean value.

Considering the overall energy distribution of H1821+643, it would be of interest to determine where the spectrum peaks: at *IUE* frequencies as suggested by the detected turnover, at soft X-ray energies as indicated by the *HEAO 1* data, or in the unobservable EUV gap. Krolik & Kallman (1988) investigated this question theoretically by modeling the effects of the several different accretion disk spectra [i.e., bare power law, power law plus disk spectrum peaking at  $10 \text{ eV}$  ( $\log \nu_0 \sim 15.4$ ), and one peaking at  $80 \text{ eV}$  ( $\log \nu_0 \sim 16.3$ )] on the emission line formation. Although the ionization parameter  $\Xi$  is far more important than the shape of the ionizing spectrum in determining the line emission, there are line ratios which are relatively insensitive to the ionization parameter.

The observed line ratios in H1821+643 are consistent with a power law plus disk spectrum peaking at  $10 \text{ eV}$ , i.e., in the UV, within the context of the Krolik & Kallman (1988) model. All ratios are within the model range (with the pressure as a free parameter between  $6.3 \times 10^{13}$  and  $20 \times 10^{13} \text{ K cm}^{-3}$ ) for the high ionization case ( $\Xi = 2.0$ ), except for C III]  $\lambda 1909$ /C IV  $\lambda 1549$  (the one ratio that is substantially smaller than the average value for Kwan & Krolik's 1981 sample of AGNs). A high  $\Xi$  might be expected for an ionizing spectrum peaking at low energies in order to produce enough high-ionization species.

### 3.4. Absorption Lines

The location of H1821+643 at  $(l, b) = (94^\circ, 27^\circ)$  and the moderate column density of  $4.1 \times 10^{20} \text{ cm}^{-2}$  are ideal for study of interstellar absorption. The Galactic longitude of H1821+643 permits optimal velocity separation of distant matter from local matter, while the low-latitude permits the viewing of distant matter at large height above the Galactic plane. Therefore, future high-resolution studies of the absorp-

TABLE 5  
ABSORPTION-LINE MEASUREMENTS OF H1821+643

ID	EW (Å)
S II $\lambda$ 1251, 1254, 1260, Si II $\lambda$ 1260 .....	0.8
O I $\lambda$ 1302, Si II $\lambda$ 1304 .....	2.6
C IV $\lambda$ 1548,51 .....	<0.7
Al II $\lambda$ 1671 .....	0.6
Fe II $\lambda$ 2343 .....	2.8
Fe II $\lambda$ 2374,2382 .....	3.5
Fe II $\lambda$ 2586 .....	1.6
Fe II $\lambda$ 2599 .....	1.8
Mg II $\lambda$ 2796,2803 .....	3.9

tion features in H1821+643 could investigate the properties of the interstellar medium at large galactocentric distances. We measured the absorption lines listed in Table 5 and indicated by tick marks in Figure 2. The lines are from low-ionization species, except for C IV for which only an upper limit is obtained due to its location on the blue wing of Lyman- $\alpha$ . The C IV  $\lambda$ 1548, 1551 absorption is thought to arise in the Galactic halo (Savage 1988). We did not detect any absorption lines in the optical spectrum. An extensive compilation of EWs of absorption lines arising at higher Galactic latitude ( $b \sim 60^\circ$ , Savage 1988) gives lower values than ours (typically by a factor of about 2) for the low-ionization species except S II, Si II and Al II. Other studies of absorption features arising at lower latitudes [( $l, b$ ) = (96°, 12°), Pettini et al. 1982] show the same strong absorption in Mg II  $\lambda$ 2796,2803 and Fe II  $\lambda$ 2599 as we measured in H1821+643.

In H1821+643, the spectral region between Lyman- $\alpha$  and C IV  $\lambda$ 1549 covers the redshift range 0.04–0.27 for detection of C IV absorption lines arising between the QSO and our Galaxy. In this sensitive part of the SWP camera no such absorption features were found above the detection threshold of EW  $\sim 0.3$  Å. The spectral region shortward of the Lyman  $\alpha$  emission line allows the detection of low-redshift Lyman  $\alpha$  forest lines. Although in the co-added SWP spectrum there are several possible absorption features in this region (e.g., at  $\lambda \sim 1470$  and 1490 Å), none were present persistently in all four SWP spectra. The absence of intergalactic Lyman- $\alpha$  and C IV lines is expected for the low redshift of H1821+643 (Bergeron 1988).

#### 4. ACCRETION DISK MODELS

Through studies of variability at different wavelengths (Cutri et al. 1985), and continuum energy distributions between IR, optical, UV, and X-rays (Malkan & Sargent 1982), it has been established that the optical/UV bump is a separate feature from the underlying power law and is now usually attributed to an accretion disk.

In the original model of Shakura & Sunyaev (1973), a summation of Planckian emission arises from the geometrically thin (but optically thick) accretion disk. At the high-frequency side a turnover occurs, corresponding to that blackbody curve with the maximal temperature at the inner disk. There are two free parameters in this model (in addition to the inclination  $i$ , and the outer radius of the disk, which affects the low-energy side): the mass  $M$  of the central black hole and the accretion rate  $\dot{M}$ . In addition, the optical continuum generally deviates from the overall power law around 3000 Å. This emission is attributed to Balmer continuum and blended Fe II line emission (Wills, Netzer, & Wills 1985).

Several modifications to the original model have been suggested: inclusion of opacity (e.g., electron scattering and Comptonization) and inclination effects (Czerny & Elvis 1987; Wandel & Petrosian 1988). The Comptonization hardens the emitted spectrum without increasing the energy requirements, and therefore keeps the luminosity sub-Eddington. One of the inclination effects is relativistic focussing of the innermost rays along the disk (Cunningham 1975), resulting in harder spectra for disks which are viewed edge-on. The effects of scattering around the disk have been modeled using stellar atmospheres (Sun & Malkan 1987), resulting in a strong Lyman limit absorption edge for disks observed face-on. However, these authors indicate that blackbody disk models fit the observations better than the models using stellar atmospheres (Sun & Malkan 1989a).

Although alternatives to the thin accretion disk models are available (e.g., the thick torus model by Madau 1988), thin disks are widely used as these have been shown to fit observations of QSOs and Seyfert 1 galaxies successfully (Malkan & Sargent 1982). We calculated disk models for a nonrotating black hole ( $a/M = 0$ , the Newtonian case), with the standard assumption that the emerging radiation can be described locally by a blackbody spectrum. The temperature  $T$  at radius  $R$  is given by

$$T(R) = \left\{ \frac{3GM\dot{M}}{8\pi\sigma R^3} \left[ 1 - \left( \frac{R_{\text{in}}}{R} \right)^{1/2} \right] \right\}^{1/4}, \quad (1)$$

where  $R_{\text{in}}$  is the innermost stable orbit ( $R_{\text{in}} = 3R_{\text{Sch}}$ , Shakura & Sunyaev 1973). We did not include relativistic effects, since the disk around a nonrotating black hole does not reach close to the black hole (unlike the case of the rotating black hole, where the disk reaches much closer) and the relativistic contributions are, therefore, relatively small. The emergent flux is calculated after fixing the inclination angle such that  $\cos i = 0.5$  and assuming a distance  $D$  given by

$$D = \frac{cz}{H_0} \left( 1 + \frac{z}{2} \right), \quad (2)$$

for  $q_0 = 0$  and  $H_0 = 50 \text{ km s}^{-1} \text{ Mpc}^{-1}$ . We did not include a fitting component to account for the Balmer continuum and blended Fe II line emission, and, therefore, our fits deviate from the observed data points between  $\log \nu_0 \sim 14.8$  and  $\log \nu_0 \sim 15.2$ .

The best-fit (by eye) to the 1987 IUE data, as shown in Figure 6, with a thin accretion disk model added to the power law, is satisfactory to explain the optical/UV spectrum with the following fitting parameters:  $M = (3 \pm 0.5) \times 10^9 M_\odot$ ,  $\dot{M} = 19 \pm 3 M_\odot \text{ yr}^{-1}$ ,  $R_{\text{out}}/R_{\text{in}} = 12(+5, -3)$ , ( $L/L_{\text{Edd}} = 0.16$ ). The fit is constrained at both the high-energy side because of the turnover of the high-frequency IUE data points and at the low-energy side due to the steep rise of optical data points. The major sources of uncertainty in the fitting parameters are (1) the nonsimultaneity of the optical and UV data points, (2) the contribution of the Balmer continuum and the Fe II lines, and (3) the correction for interstellar reddening. In this model, the mass of the central object determines mainly the frequency of the peak, while the accretion rate determines mostly the normalization. Once these two parameters have been determined by the turnover in the UV and the strength of the optical/UV bump, respectively, the width of the bump is determined by the extent of the disk, i.e., the ratio  $R_{\text{out}}/R_{\text{in}}$ . The lower limit to  $R_{\text{out}}/R_{\text{in}}$  rules out the possibility of a single blackbody fit, which

would result in a far too narrow bump. If the reality of the UV turnover seen around  $\log \nu_0 = 15.3$  is doubted, then the bump could peak at higher frequencies, outside the range of *IUE*. In that case,  $M$  would be smaller and the bump would be wider requiring a larger disk (possibly increasing  $R_{\text{out}}/R_{\text{in}}$  to about 30). Such a result is within the range of acceptable fits to the 1989 June *IUE* data, as the short-wavelength turnover is not apparent then. To estimate the uncertainty due to the interstellar reddening correction, we found that  $E(B-V) = 0.1$  mag (an increase by about 20%), would increase  $\dot{M}$  by about 10%, while  $M$  and the size of the disk would remain unchanged. The use of a color excess of  $E(B-V) = 0.12$  mag or higher would result in a dereddened spectrum without a turnover, again increasing the uncertainty in  $M$  and  $R_{\text{out}}/R_{\text{in}}$ . However, such a large color excess would correspond to a hydrogen column density of  $5.8 \times 10^{20} \text{ cm}^{-2}$ , far above the values measured near H1821+643.

The novel result of this analysis is the relatively small value of  $R_{\text{out}}/R_{\text{in}}$  (9–17). Bechtold et al. (1987) applied a similar fitting model to the spectrum of PG 1211+143 and found a best fit  $R_{\text{out}}/R_{\text{in}}$  of at least 200, considerably larger than we found in H1821+643. It is of interest to note that the unexpectedly small outer radius in H1821+643 could be identified with the maximum or critical radius ( $R_{\text{crit}}$ ) in the so-called two-temperature accretion flow model of Begelman, Sikora, & Rees (1987). These authors studied the ion torus around a central black hole, and in particular, the cooling effects of electron-positron pair production on such a torus. Due to these cooling effects the torus collapses to a geometrically thin, optically thick annulus in the innermost region, defined by  $R < R_{\text{crit}} \sim 30 R_{\text{Sch}}$ . The thermal UV and possibly the soft X-rays would come from this optically thick region, which would in fact have an outer radius remarkably close to our fit value  $R_{\text{out}} = 36 R_{\text{Sch}}$  ( $R_{\text{out}}/R_{\text{in}} = 12$ ). In this model, due to the bistability of the annulus, smooth changes in  $\dot{M}$  would cause abrupt changes in the flow structure, which in turn would be responsible for spectral variations. In a stable disk, changes in  $\dot{M}$  would affect the emergent spectrum only on the viscosity time scale  $t_{\text{vis}}$  (Bechtold et al. 1987); for an  $\alpha$  disk with the parameters inferred for H1821+643 above,  $t_{\text{vis}}$  is greater than 6000 yr for  $\alpha < 1.0$  (Frank, King, & Raine 1985).

A successful fit of both the optical/UV bump and the *HEAO 1* soft X-ray excess is practically impossible to achieve, considering the decline of the *IUE* data points, and the high and fairly constant flux level for the 0.5–2 keV *HEAO 1* observations. If such a fit is forced (ignoring the nonsimultaneity of the UV and X-ray data), highly super-Eddington luminosities ( $L \sim 40 L_{\text{edd}}$ ) would be produced for the Newtonian accretion disk models, violating the thin disk approximation for the inner disk (Bechtold et al. 1987), unless Compton scattering of the UV photons to EUV and soft X-ray energies is incorporated (Czerny & Elvis 1987). While following the optical data points rather closely, such a fit exceeds the observed UV flux by a factor of about 2–3. Moreover, as there is no evidence that the UV emission and the soft X-ray excess are linked in AGNs (Elvis, Wilkes, & McDowell 1989), there is no convincing justification to fit both features in one model fit for H1821+643 at this moment. This QSO would, however, be an excellent candidate to study whether the UV and soft X-ray radiation have the same physical origin, considering the variability and brightness of both the UV and X-ray emission. In Figure 4 the change in the UV continuum over a period of 4 months is shown. This change in shape, where the spectral hardness is

correlated with luminosity, is often found in AGNs which are well observed with *IUE* (Edelson, Krolik, & Pike 1990) and is consistent with an expected increase of temperature with accretion rate. The reported minimum doubling time of about 10 days at X-ray energies (Snyder & Wood 1984) could be identified with the dynamical time scale ( $t_{\text{dyn}}$ ) of the inner disk. We define  $t_{\text{dyn}}$  as  $(1+z) R_{\text{max}}/v_{\text{max}}$ , where  $R_{\text{max}}$  is the radius at which the temperature of the disk reaches a maximum ( $R_{\text{max}} \sim 8GM/c^2$ ) and  $v_{\text{max}} = (GM/R_{\text{max}})^{1/2}$ . Thus,  $t_{\text{dyn}} = GM(8/c^2)^{3/2} (1+z)$  as seen by the observer, or  $t_{\text{dyn}} \sim 1.7 (M/10^9 M_{\odot})$  days.

Sun & Malkan (1989a) presented fits of a thin accretion disk model to the spectra of 24 AGNs, not including H1821+643. As the inferred disk parameters are very similar in the Schwarzschild metric (used by Sun & Malkan 1989a) and the Newtonian metric (used here) for  $\cos i = 0.5$ , we can compare our values obtained for mass and accretion rate with the large sample. With  $M = 3 \times 10^9 M_{\odot}$ , H1821+643 would be one of the most massive AGNs in the sample and the most massive of the AGNs with intermediate redshift ( $z = 0.2$ – $1.0$ ). The inferred accretion rate of  $\dot{M} = 19 M_{\odot} \text{ yr}^{-1}$  would be one of the highest for an intermediate redshift QSOs. This was to be expected, considering the large luminosity of H1821+643 and the pronounced optical/UV bump in its spectrum.

There is, however, one significant difference between our model and that of Sun & Malkan (1989a), and that is the use of the outer radius of the accretion disk. Sun & Malkan (1989a) do not specify their outer radius, but it can be assumed to be a large value. In our fitting model the outer radius is a free parameter, resulting typically in low inferred values for successful fits ( $R_{\text{out}}/R_{\text{in}} \sim 12$ ). A strong UV/optical bump with a small width, as is the case for H1821+643, can only be fitted in a satisfactory manner with a small accretion disk. While the turnover and the height of the UV bump determine the central mass and accretion rate, the extent of the disk is determined by the width of the bump. We maintain that only a limited disk, in which the range of temperatures is small and therefore the emergent spectrum only slightly broader than the single blackbody curve, fits a narrow optical/UV bump, as observed in H1821+643.

## 5. CONCLUSIONS

We have obtained multiwavelength observations of H1821+643 and have modeled its continuum with an accretion disk in addition to an underlying power law. The continuum follows the power law with  $\alpha = 1.16$  most closely in the far-IR and near-IR, deviating strongly at optical and UV frequencies, and possibly at soft X-ray energies. Most of the energy is emitted in the UV, while the variable soft X-ray excess could have a similar luminosity when at maximum. Fits with a geometrically thin, optically thick accretion disk yield a central black hole mass of  $3 \times 10^9 M_{\odot}$  and an accretion rate of  $19 M_{\odot} \text{ yr}^{-1}$ , both large values consistent with the luminosity of H1821+643 and the prominence of the optical/UV bump in its continuum spectrum. The accretion disk fits result in a surprisingly small disk size ( $R_{\text{out}}/R_{\text{in}} = 12$ ). Efforts to constrain the extreme UV spectrum by applying photoionization models, which predict emission line ratios, were indicative of an ionizing spectrum peaking at UV frequencies.

The shape of the UV continuum spectrum was found to vary significantly, but the time scale of the UV variability remains to be determined by periodic observations. An outstanding question for QSOs with both a strong optical/UV bump and a soft



X-ray excess, of which H1821+643 is a prime example, is whether these components have a common origin. Simultaneous observations at UV and soft X-ray frequencies could determine whether both features are present at the same time. If both emissions arise in an accretion disk, then this should be reflected in the continuum energy distribution and the correlated variability of the UV and soft X-ray flux. To fit both the UV bump and the soft X-ray excess as one feature seems problematic in the current accretion disk models (e.g., requiring highly inclined disks around rapidly rotating holes, as shown by Sun & Malkan 1989a, or the inclusion of a strong Comptonized component, as calculated by Czerny & Elvis 1987). H1821+643, with its strong emission in all wavelength bands (except radio), and its variability in the UV and soft

X-ray flux, is an outstanding candidate for simultaneous monitoring in the X-ray and the UV band.

We acknowledge the able assistance of the staff at the Goddard *IUE* Regional Data Analysis Facility. We thank Martin Elvis and Saeqa Vrtiliek for obtaining the infrared and optical magnitudes, respectively. This research was supported by NASA *IUE* grants NAG 5-1140 and NAG 5-1425 to the Columbia Astrophysics Laboratory. A. V. F. is supported by NASA grant NAG 5-1171, as well as by NSF grants AST-8957063 and AST-9003829. Lick Observatory is partially funded by NSF Core Block grant AST-8614510. This paper is contribution number 432 of the Columbia Astrophysics Laboratory.

## REFERENCES

- Bechtold, J., Czerny, B., Elvis, M., Fabbiano, G., & Green, R. F. 1987, *ApJ*, 314, 699
- Begelman, M. C., Sikora, M., & Rees, M. J. 1987, *ApJ*, 313, 689
- Bergeron, J. 1988, in *QSO Absorption Lines*, ed. J. C. Blades, D. Turnshek, & C. A. Norman (Cambridge: Cambridge University Press), p. 127
- Bohlin, R. C., Savage, B. D., & Drake, J. F. 1978, *ApJ*, 224, 132
- Cunningham, C. T. 1975, *ApJ*, 202, 788
- Cutri, R. M., Wisniewski, W. Z., Rieke, G. H., & Lebofsky, M. J. 1985, *ApJ*, 296, 423
- Czerny, B., & Elvis, M. 1987, *ApJ*, 321, 305
- Edelson, R. A., Krolik, J. H., & Pike, G. F. 1990, *ApJ*, 359, 86
- Edelson, R. A., & Malkan, M. A. 1986, *ApJ*, 308, 59
- Elvis, M. 1988, in *Supermassive Black Holes*, ed. M. Kafatos (Cambridge: Cambridge University Press), p. 131
- Elvis, M., Wilkes, B. J., & McDowell, J. C. 1989, in *Extreme Ultraviolet Astronomy*, ed. R. F. Malina & S. Bowyer (New York: Pergamon)
- Filippenko, A. V. 1982, *ASP*, 94, 715
- Frank, J., King, A. R., & Raine, D. J. 1985, in *Accretion Power in Astrophysics* (Cambridge: Cambridge University Press), p. 101
- Grauer, A. D., & Bond, H. E. 1984, *ApJ*, 277, 211
- Kii, T., et al. 1991, in *ApJ*, in press.
- Kinney, A. L., Huggins, P. J., Bregman, J. N., & Glassgold, A. E. 1985, *ApJ*, 291, 128
- Kriss, G. A. 1988, *ApJ*, 324, 809
- Krolik, J. H., & Kallman, T. R. 1988, *ApJ*, 324, 714
- Kwan, J., & Krolik, J. H. 1981, *ApJ*, 250, 478
- Madau, P. 1988, *ApJ*, 327, 116
- Malkan, M. A., & Sargent, W. L. W. 1982, *ApJ*, 254, 22
- Marshall, F. E., Boldt, E. A., Holt, S. S., Mushotsky, R. F., Pravdo, S. H., Rothschild, R. E., & Serlemitsos, P. J. 1979, *ApJS*, 40, 657
- Massey, P., Strobel, K., Barnes, J. V., & Anderson, E. 1988, *ApJ*, 328, 315
- Miller, J. S., & Stone, R. P. S. 1987, the CCD Cassegrain Spectrograph at the Shane Reflector (Lick Observatory Technical Report No. 48, Santa Cruz, CA)
- Neugebauer, G., Miley, G. K., Soiffer, B. T., & Clegg, P. E. 1986, *ApJ*, 308, 815
- Nugent, J. J., et al. 1983, *ApJS*, 51, 1
- Oke, J. B., & Gunn, J. E. 1983, *ApJ*, 266, 713
- Pettini, M., et al. 1982, *MNRAS*, 199, 409
- Pravdo, S. H., & Marshall, F. E. 1984, *ApJ*, 281, 570
- Reichert, G. A., Polidan, R. S., Wu, C.-C., & Carone, T. E. 1988, *ApJ*, 325, 671
- Savage, B. D. 1988, in *QSO Absorption Lines*, ed. J. C. Blades, D. Turnshek, & C. A. Norman (Cambridge: Cambridge University Press), p. 195
- Scott, H. A., & O'Dell, S. L. 1989, in *IAU Symposium 134, Active Galactic Nuclei*, ed. D. E. Osterbrock & J. S. Miller (Dordrecht: Reidel), p. 257
- Seaton, M. J. 1979, *MNRAS*, 187, 73P
- Shakura, N. I., & Sunyaev, R. A. 1973, *A&A*, 24, 337
- Snyder, W. A., & Wood, K. S. 1984, in *X-ray and UV Emission from Active Galactic Nuclei*, ed. W. Brinkman & J. Truemper (Garching: Max Planck Institut), p. 114
- Stark, A. A., Heiles, C., Bally, J., & Linke, R. 1990, in preparation
- Sun, W.-H., & Malkan, M. A. 1987, in *Astrophysical Jets and Their Engines*, ed. W. Kundt (Dordrecht: Reidel), p. 125
- . 1989a, *ApJ*, 346, 68
- . 1989b, in *IAU Symposium 134, Active Galactic Nuclei*, ed. D. E. Osterbrock & J. S. Miller (Dordrecht: Reidel), p. 262
- Turner, M. J. L., et al. 1989, in *Proceedings of 23d ESLAB Symp.* (Noordwijk, The Netherlands: ESA Publ.), p. 769
- Wandel, A., & Petrosian, V. 1988, *ApJ*, 329, L11
- Warwick, R. S., Barstow, M. A., & Yaqoob, T. 1989, *MNRAS*, 238, 917
- Wills, B. J., Netzer, H., & Wills, D. 1985, *ApJ*, 288, 94
- Wood, K. S., et al. 1984, *ApJS*, 56, 507